

On the Effect of Muscular Co-contraction on the 3D Human Arm Impedance

Harshil Patel, Gerald O'Neill, and Panagiotis Artemiadis*

Abstract—Humans have the inherent ability to performing highly dexterous tasks with their arms, involving maintenance of posture, movement, and interaction with the environment. The latter requires the human to control the dynamic characteristics of the upper limb musculoskeletal system. These characteristics are quantitatively represented by inertia, damping, and stiffness, which are measures of mechanical impedance. Many previous studies have shown that arm posture is a dominant factor in determining the end point impedance on a horizontal plane. This paper presents the characterization of the end point impedance of the human arm in three-dimensional space. Moreover, it models the regulation of the arm impedance with muscle co-contraction. The characterization is made by route of experimental trials where human subjects maintained arm posture while their arms were perturbed by a robot arm. Furthermore, the subjects were asked to control the level of their arm muscles' co-contraction, using visual feedback, in order to investigate the effect of muscle co-contraction on the arm impedance. The results of this study show an anisotropic increase of arm stiffness due to muscle co-contraction. These results could improve our understanding of the human arm biomechanics, as well as provide implications for human motor control – specifically the control of arm impedance through muscle co-contraction.

Index Terms—arm impedance, muscle co-contraction, exoskeleton control

I. INTRODUCTION

The wide range of applications involving physical interaction of robots with humans has received increased attention in the last decades. Since the late 80's, there has been a substantial amount of interest in measuring human arm two dimensional (2D) end-point stiffness characteristics, where the arm is supported and constrained to movement within a horizontal (transverse) plane. A perturbation method for measuring hand stiffness was developed by using a manipulandum to displace the subject's hand during maintenance of a given posture in [1]. Stiffness values were represented both numerically and graphically, using ellipses. These showed that the human musculoskeletal system has spring-like properties that enable posture stabilization and interaction with the environment.

From a technological point of view, many different apparatuses have been used for identifying dynamic properties of the human upper limbs, ranging from mechanical linkages that are aligned with the anatomical joints [2], to manipulanda that are held by the subject's end-effector [3]–[5]. The perturbation method for estimating arm stiffness has been used

by many other studies as well [6]–[9]. In [10] and [11], the perturbation method was extended to include measurement of other dynamic components: inertia and damping in addition to stiffness. However, all these studies focus on the identification of the impedance components in 2D, which limits the range of application. The first attempt to characterize arm impedance in three-dimensional (3D) space was described in [12], while the characterization of arm stiffness in 3D space has been also studied in [13]. The effect of arm posture on the arm stiffness characteristics has been also studied for a single endpoint position, using subject-selected arm configuration in [14], [15].

Although most of the past studies have focused on perturbations during maintained hand posture, there are a few studies that focused on the effect of muscle activation on the arm stiffness [6], [16]–[22]. Two degrees of freedom were usually investigated, single endpoint positions, involving a small number of muscles. Control of arm stiffness by co-activating muscles provides the ability to safely interact with the environment for every-day-life tasks. Therefore, the investigation of the control principles for the voluntary adjustment of arm stiffness is quite significant, and so far unexplored. The latter is the rationale of our study.

In this paper, a systematic method for characterizing human arm impedance in 3D space and its regulation through muscle co-contraction is presented. A 7 degrees-of-freedom (DoFs) robot arm is used to impose motion to, and measure interaction forces from, a human subject's arm. The subject's arm is appropriately coupled to the robot's end-effector and is perturbed along the three axes starting from 7 different points, each corresponding to a different arm configuration in 3D space. All the perturbations are repeated for four cases, each involving a different level of muscle co-contraction. A simplified linear model for impedance is used to characterize inertia, damping and stiffness using measured motion and force data for the 4 cases of muscle co-contraction. The stiffness characteristics are described using ellipsoids, and the effect of arm configuration and muscle co-contraction to the stiffness ellipsoids is investigated.

II. MATERIALS AND METHODS

A. Apparatus

The subjects were seated on a chair placed next to a 7-DoF robot arm (LWR4+, KUKA). They were strapped to the chair and their right arm was coupled to the robot arm via a mechanical coupling, attached to the end-effector of the robot arm as shown in Fig.1A. The mechanical coupling is designed such that it allows no axial or rotational movement

Harshil Patel, Gerald O'Neill, and Panagiotis Artemiadis are with the Mechanical and Aerospace Engineering program, Ira A. Fulton Schools of Engineering, Arizona State University, Tempe, Arizona 85287 email: {hpatel5, goneill, panagiotis.artemiadis}@asu.edu.

* Corresponding author.

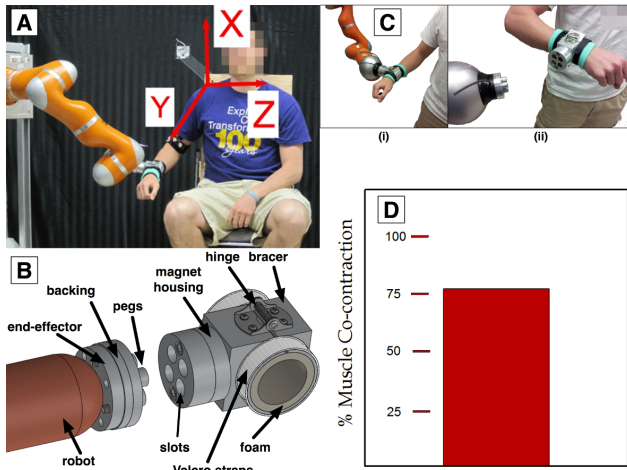


Fig. 1. (A) Experimental setup: The robot arm is interfaced with the subject's forearm through the mechanical coupling attached at the end-effector. Position tracking sensors are placed adjacent to the robot base and subject's shoulder defining two reference systems. EMG electrodes are placed on 6 muscles of the shoulder and elbow. Chair straps are not shown in the picture, but they were used during the experiments. (B) Coupling components at the human side (right) and the robot side (left). (C) i) Human-robot coupled configuration, ii) Uncoupled configuration. (D) Visual display indicating the muscle co-contraction index.

of the lower arm inside it, since it is attached to the human forearm close to the wrist [23]. The coupling insured that there was no kinematic redundancy in the subject's arm for any configuration. The coupling components as well as the way the human is coupled-decoupled from the robot using the device are shown in Fig. 1B and 1C respectively. Muscle activation was measured through wireless surface electromyography (EMG) electrodes (Trigno Wireless, Delsys). Since the focus is arm impedance, and the coupling is on the forearm, the muscles that contribute to shoulder and elbow impedance were recorded: Anterior Deltoid (AD), Posterior Deltoid (PD), Pectoralis Major (PM), Trapezius (T), Biceps Brachii (BB) and Triceps Longus (TL).

B. Procedure and Tasks

Four subjects, all male ranging in age from 20 to 26 years, three of them right handed and one left handed, participated in this experiment. As explained above, the subjects were strapped onto a seat placed next to the robot arm. Seven different end-effector poses (position and orientation) in the robot workspace were selected. With the subject strapped in the same position on the chair and their right hand coupled to the end-effector, each of these start points $S^{(i)} : i = 1, 2, \dots, 7$ corresponded to a specific configuration of the subject's arm. The seven arm configurations tested spanned a wide range of arm positions in 3D space, as shown in Fig. 2. The robot was controlled to impose perturbations in 18 different directions in 3D space. This was done by controlling the robot to move to 18 equally-spaced points $P_j^{(i)}, j = 1, \dots, 18$ that lie on a sphere with a center of the corresponding $S^{(i)}$ point, and a radius of 8mm. The motion of the robot from $S^{(i)}$ to each one of the 18 $P_j^{(i)}$ points lasted 100ms, and corresponded to the robot-induced perturbation to the human arm. Once the robot arrives

at $P_j^{(i)}$, it remains stationary for 500ms and then returns back to $S^{(i)}$. After a resting phase of 1s, the robot is commanded to reach the next $P_j^{(i)}$ point, and the procedure is repeated for all the 18 $P_j^{(i)}$ points. The trajectory of the robot motion along each axis was designed using a 3rd order polynomial function. The robot provided feedback of the joint angles, as well as end-effector forces at a frequency of 1000Hz.

Prior to performing the experiment, the subjects were asked to co-contrast their arm muscles to their maximum ability, while their arm was in one of the 7 configurations selected (configuration 5). EMG signals were recorded from the six muscles mentioned above and sampled at a frequency of 1000Hz. The signals were then full-wave rectified and low-pass filtered (2nd order Butterworth filter, cut-off frequency of 8 Hz). The processed signals $e_m, m = 1, \dots, 6$ were stored, and the maximum values for each muscle $e_{m,max}$ were computed in order to be used as normalization factors for the experiments. During the perturbation experiments the total co-contraction index C was computed in real-time based on the individual muscle normalized activation level with respect to their maximum activation level $e_{m,max}$. Therefore, the co-contraction index was given by:
$$C = \frac{1}{6} \sum_{m=1}^6 \frac{e_m}{e_{m,max}}$$

The robot-induced perturbation experiments were grouped into four cases. In each case, the subject was asked to maintain a certain co-contraction level of his muscles. The robot-induced perturbations were identical across the four cases. The co-contraction index C was computed in real-time based on the muscles' activation, and was displayed to the subject in the form of a bar graph, as shown in Fig. 1D. The visual display was shown on a monitor placed in front of the subject, and was updated at a frequency of 1000Hz. The levels of co-contraction that the subjects we asked to maintain were 0%, 50%, 75% and 100% for the four phases respectively. For each of the 7 arm configurations, the robot perturbation phase was divided into three sets of 6 perturbations each, thereby providing enough time for the subject to relax his muscles and limiting possible muscle fatigue.

C. Data Processing

As explained earlier, the goal of the study is to investigate how arm impedance changes as a function of muscle co-contraction. The arm impedance characteristics - inertia, damping and stiffness - are characterized using a linear model describing the relationship between measured opposing forces and position of the arm.

During the experiment, the arm is coupled to the end-effector of the robot arm via the mechanical coupling. The position of the end point of the arm, a point in the forearm, was defined as the center point of the cylindrical housing of the mechanical coupling. Since the coupling was attached to the robot arm, the 3D position of this point was tracked at each instance through the robot joint angles after applying the forward kinematic equations of the robot arm. Therefore, all the motion profiles and end-effector forces were obtained with respect to the robot base reference system $\langle X_R, Y_R, Z_R \rangle$. Using homogeneous transformation between the robot and

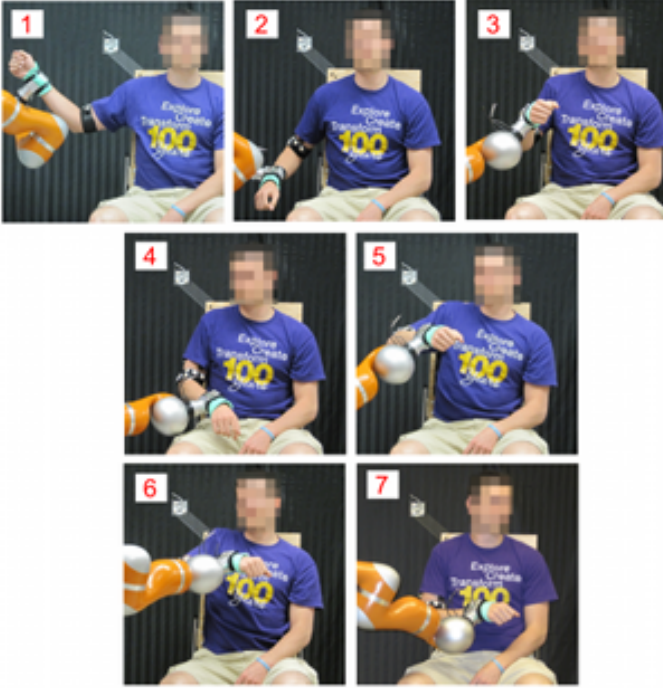


Fig. 2. The 7 configurations of the arm used.

the robot mounting plate reference system $\langle X_B, Y_B, Z_B \rangle$, the position of the human end-point, and the interaction forces, were computed with respect to the human-centered reference frame $\langle X, Y, Z \rangle$.

As mentioned earlier, the robot-induced perturbations lasted for 100ms. For all cases (0%, 50%, 75%, 100% co-contraction) we used force and position data collected during those 100ms of perturbation in order to estimate the arm impedance. Although the mechanical perturbations might evoke muscle reflex responses, the characterization of the effect of the latter on the arm impedance is out of the scope of this paper. In fact, in most cases of human-environment interaction, where impedance adjustment is necessary, muscle reflexes are going to be present and affect arm dynamics. Therefore, since a realistic-practical model of the effect of muscle co-contraction on arm impedance is the main focus of this study, we decided to include any reflex responses – and their effects – in our impedance estimates.

D. Impedance estimation

The force and motion profiles of interest, i.e. during the 100ms robot-induced perturbations were extracted for processing. The initial values of forces (average values along 30ms before the perturbation onset) in all directions were subtracted from the subsequent force profiles. This ensured that any kind of sensor offset or gravitational forces due to weight of the arm did not affect the opposing force measurements. Since length and duration of the perturbations were very small, the model of the end point impedance can be expressed by the following equation:

$$\mathbf{F} = \mathbf{I}\ddot{\mathbf{X}} + \mathbf{B}\dot{\mathbf{X}} + \mathbf{K}\mathbf{X} \quad (1)$$

where \mathbf{I} , \mathbf{B} and \mathbf{K} represent the 3×3 arm inertia, damping and stiffness matrices respectively. $\ddot{\mathbf{X}}$, $\dot{\mathbf{X}}$ and \mathbf{X} are the 3D acceleration, velocity and displacement vectors respectively, while \mathbf{F} is the 3D vector of opposing forces. All variables are expressed with respect to the human-centered reference frame $\langle X, Y, Z \rangle$. Equation (1) can be re-written in a parameter identification form as shown below:

$$\mathbf{F} = \mathbf{P}\mathbf{Y} \quad (2)$$

where $\mathbf{F} = [F_x \ F_y \ F_z]^T$, $\mathbf{Y} = [\ddot{\mathbf{X}}^T \ \dot{\mathbf{X}}^T \ \mathbf{X}^T]^T$ and \mathbf{P} is a 3×9 impedance matrix to be identified, given by $\mathbf{P} = [\mathbf{I} \ \mathbf{B} \ \mathbf{K}]$ where \mathbf{I} is the inertia matrix, \mathbf{B} is the damping matrix, and \mathbf{K} is the stiffness matrix defined by:

$$\mathbf{I} = \begin{bmatrix} I_{xx} & I_{xy} & I_{xz} \\ I_{yx} & I_{yy} & I_{yz} \\ I_{zx} & I_{zy} & I_{zz} \end{bmatrix} \quad \mathbf{B} = \begin{bmatrix} B_{xx} & B_{xy} & B_{xz} \\ B_{yx} & B_{yy} & B_{yz} \\ B_{zx} & B_{zy} & B_{zz} \end{bmatrix} \\ \mathbf{K} = \begin{bmatrix} K_{xx} & K_{xy} & K_{xz} \\ K_{yx} & K_{yy} & K_{yz} \\ K_{zx} & K_{zy} & K_{zz} \end{bmatrix} \quad (3)$$

Using n data points for opposing force and position measurements collected from the experiments, the impedance matrix \mathbf{P} was computed using linear regression method given by the following:

$$\mathbf{P} = \mathbf{F}_N \mathbf{Y}_N^\dagger \quad (4)$$

where \mathbf{Y}_N^\dagger is the right pseudo-inverse matrix of \mathbf{Y}_N [24]. \mathbf{F}_N and \mathbf{Y}_N were computed by concatenating n instances of \mathbf{F} and \mathbf{y} respectively as follows:

$$\mathbf{F}_N = [\mathbf{F}_1 \cdots \mathbf{F}_n], \quad \mathbf{Y}_N = [\mathbf{Y}_1 \cdots \mathbf{Y}_n] \quad (5)$$

The impedance matrices \mathbf{I} , \mathbf{B} and \mathbf{K} were separated into symmetric and antisymmetric matrix components. Generally any 3×3 matrix \mathbf{Z} can be separated into the symmetric $\mathbf{Z}^{(S)}$ and anti-symmetric component $\mathbf{Z}^{(A)}$ as follows [25]:

$$\mathbf{Z} = \begin{bmatrix} Z_{xx} & Z_{xy} & Z_{xz} \\ Z_{yx} & Z_{yy} & Z_{yz} \\ Z_{zx} & Z_{zy} & Z_{zz} \end{bmatrix} = \mathbf{Z}^{(S)} + \mathbf{Z}^{(A)} \quad (6)$$

where

$$\mathbf{Z}^{(S)} = \frac{1}{2}(\mathbf{Z} + \mathbf{Z}^T), \quad \mathbf{Z}^{(A)} = \frac{1}{2}(\mathbf{Z} - \mathbf{Z}^T). \quad (7)$$

III. RESULTS

A. Co-Contraction Index

Before analyzing the impedance characteristics identified for the various levels of muscle co-contraction, it is worth investigating the ability of the human subjects to control their muscles' activation, based on the visual feedback of the co-contraction index introduced above. Fig. 3 shows the co-contraction index when the subject was instructed to maintain it at 50%, 75% and 100% level respectively. It can be seen that the subject was able to maintain the specific level of muscle co-contraction in each case. These indexes were seen to slightly vary across the 7 configurations indicating that the ability to co-contrast the muscles to the specific level of co-contraction was different for different arm configurations.

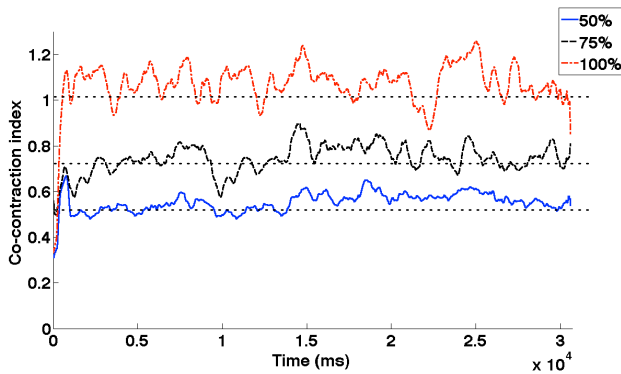


Fig. 3. Co-contraction index C for three muscle co-contraction levels 50%, 75% and 100%. A similar trend of maintaining the co-contraction index was seen for all the subjects.

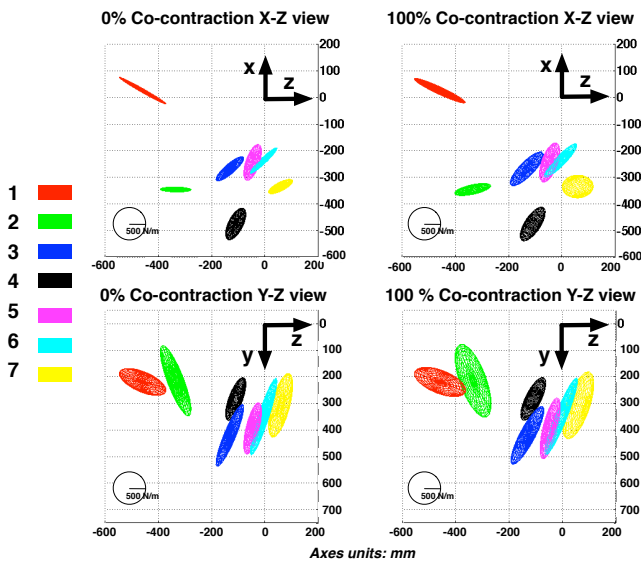


Fig. 4. Stiffness ellipsoids for a representative subject. Check Fig. 1A and 2 for axes and configurations. The 7 different configurations are color-coded on the left.

However, we chose to define the co-contraction index with respect to maximum voluntary co-contraction in a *single* arm configuration. Although we could use maximum voluntary co-contraction for each configuration tested, we decided to use only one in order to have a more general idea of the muscle co-contraction level that could generalize across configurations. This would allow further investigation of the ability of muscles to co-contraction without being limited on the arm configuration. Configuration 5 was selected because it was approximately in the mid-range of the 3D arm workspace we used.

B. Impedance matrices

The impedance matrices \mathbf{I} , \mathbf{B} and \mathbf{K} for each of the arm configurations were identified and separated into the symmetric and antisymmetric components as described in the previous section. It was observed that the opposing forces due to inertia (\mathbf{I}) and damping (\mathbf{B}) were very small compared to the ones due to arm stiffness, especially in the cases involving muscle co-contraction. For that reason, it is not

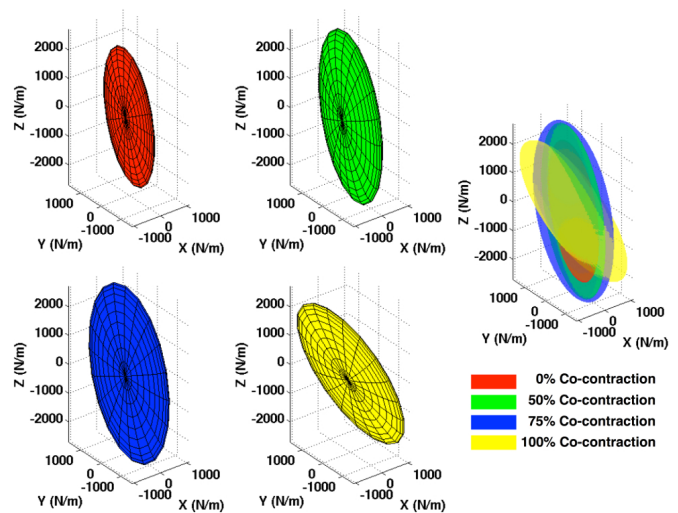


Fig. 5. Effect of muscle co-contraction on stiffness ellipsoid for an indicative case (configuration 1, subject 1).

certain that they were accurately identified using the least-squares equation. Moreover, we don't expect the inertia of the arm to vary for different muscle co-contraction levels, and there is no evidence from the literature that damping would also change with muscle co-contraction, especially given isometric conditions we investigate here [8], [9], [15]. Therefore, following directions also found in the literature [1], [7], we decided to analyze the effect of co-contraction only on arm stiffness.

The diagonal elements of the identified arm stiffness \bar{K}_{xx} , \bar{K}_{yy} , \bar{K}_{zz} , averaged across all subjects, are listed in Tables I, II, III, and IV for the different co-contraction levels 0%, 50%, 75% and 100% respectively. Moreover, the maximum of all off-diagonal elements of the anti-symmetric components are also listed. Finally the stiffness was represented as an ellipsoid in 3D space. The length of each of the primary, secondary, and tertiary axes of the ellipsoid is also listed in those tables, as \bar{K}_1 , \bar{K}_2 and \bar{K}_3 respectively. Fig. 4 shows the stiffness ellipsoids, for one of the subjects, across all 7 configurations, for 0% and 100% muscle co-contraction.

IV. DISCUSSION

In this study we focused on two main mechanisms that humans use to control arm stiffness: change of arm configuration and co-contraction of muscles. We tested those mechanisms in 7 different configurations, at 4 different co-contraction levels, in order to study their effect on arm stiffness. The effect of muscle co-contraction on the shape and orientation of the stiffness ellipsoid for an indicative case (configuration 1, subject 1) is shown in Fig. 5.

The results show that there is a statistically significant ($p \leq 0.05$) effect of both the arm configuration and the muscle activation level on arm stiffness (see values in Tables I, II, III and IV). Focusing on arm configuration, the range of stiffness values we estimated is very close to those reported in the literature for the 2D case [6]–[9]. Moreover, the antisymmetric components of the stiffness were observed to be much lower

then the symmetric components ($p \leq 0.05$) (compare fourth column of Tables I, II, III and IV with symmetric components), which agrees with the literature for planar arm configurations [1], indicating conservative force fields for the human arm in 3D space.

Of most importance, however, is the relationship between the stiffness ellipsoids and muscle co-contraction. Fig. 6 shows how the stiffness ellipsoid axes were changed in length due to muscle co-contraction for each arm configuration. All results are reported with respect to the axes of that ellipsoid, in order to quantify the effect of muscle co-contraction on the relaxed-arm stiffness characteristics. Absolute values of stiffness increase are listed in addition to percentages, in order to show that the structure-eccentricity of the ellipsoids was not changed, even when muscles were co-contracted at 100%. As it can be seen, muscle co-contraction did not change the order of the 3 axes of the ellipsoids, therefore did not affect the eccentricity of the original ellipsoid representing the relaxed muscle case. However, the increase of the length of the original axes is anisotropic, with the muscle co-contraction having the most significant effect on the secondary and tertiary axes.

Table V shows the rotation of the stiffness ellipsoids due to muscle co-contraction. More specifically, Table V reports the angle difference of each of the ellipsoid axes, for the 100% co-contraction case with respect the 0% case. $\Delta\theta_1$, $\Delta\theta_2$ and $\Delta\theta_3$ correspond to the angle difference of the primary, secondary and tertiary axes of the ellipsoids respectively, between the 0% and 100% co-contraction cases. Reported values are averaged across subjects. In terms of rotation of the ellipsoids, a 100% muscle co-contraction rotates the secondary and tertiary axes by 22.9° in average, compared to the 0% co-contraction case, while for only 7.5° in average in the case of the primary axis. Statistical analysis of all stiffness changes was done, and all changes (both in magnitude and rotation) were proved to be statistically significant ($p \leq 0.05$).

From the observations above we can conclude that muscle co-contraction induces an anisotropic change of the arm stiffness, affecting primarily the secondary and tertiary axes of the ellipsoids, and not the primary axis. A possible explanation of this phenomenon is the way individual muscles contribute to the change of the overall arm stiffness, which is a function of both the configuration of the arm, as well as the properties of each muscle independently. A further investigation of the geometry of the musculoskeletal models, as well as the contribution of each muscle to the overall arm Cartesian stiffness should be conducted. However, it is worth noting that the results are very consistent across subjects ($p \leq 0.05$).

V. CONCLUSIONS

In this paper, a systematic method for characterizing the human arm impedance in 3D space and its regulation through muscle co-contraction is presented. The proposed method is based on robot-induced perturbations in posture maintenance scenarios, however it introduces control of muscle co-contraction level by the human subject, through visual feedback. A simplified linear model for impedance is used to characterize arm stiffness using the measured motion and

force data for 4 cases of muscle co-contraction (0%, 50%, 75% and 100%). The stiffness characteristics are described using ellipsoids, and the effect of arm configuration and muscle co-contraction on the stiffness ellipsoids is investigated.

The main novelty of this paper is that it succeeds in characterizing human arm impedance in 3D space, while investigating the control humans have over the arm stiffness using muscle co-contraction. The method was applied to 4 human subjects, across whom the results were very consistent. Based on the results, we can conclude that muscle co-contraction induces an anisotropic change of the arm stiffness ($p \leq 0.05$), affecting primarily the secondary and tertiary axes of the ellipsoids, and not the primary axis. A definite explanation of this phenomenon requires further investigation, including a musculoskeletal model of the arm in order to quantify the role of the individual muscles in the overall end-point Cartesian impedance. This study can potential provide a plethora of implications for EMG-based control of robots that physically interact with humans. More specifically, understanding the voluntary control of arm impedance in task (i.e. Cartesian) space is beneficial for a plethora of applications, ranging from powered orthotics (exoskeletons), to assistive devices and rehabilitation robotics.

REFERENCES

- [1] F. A. Mussa-Ivaldi, N. Hogan, and E. Bizzi, "Neural, mechanical, and geometric factors subserving arm posture in humans," *J Neurosci*, pp. 2732–2743, 1985.
- [2] S. H. Scott, "Apparatus for measuring and perturbing shoulder and elbow joint positions and torques during reaching," *Journal of neuroscience methods*, vol. 89, no. 2, pp. 119–127, 1999.
- [3] A. M. Acosta, R. F. Kirsch, and E. J. Perreault, "A robotic manipulator for the characterization of two-dimensional dynamic stiffness using stochastic displacement perturbations," *Journal of Neuroscience Methods*, vol. 102, no. 2, pp. 177–186, 2000.
- [4] I. S. Howard, J. N. Ingram, and D. M. Wolpert, "A modular planar robotic manipulandum with end-point torque control," *Journal of neuroscience methods*, vol. 181, no. 2, pp. 199–211, 2009.
- [5] L. Masia, G. Sandini, and P. Morasso, "A novel mechatronic system for measuring end-point stiffness: Mechanical design and preliminary tests," in *Rehabilitation Robotics (ICORR), 2011 IEEE International Conference on*. IEEE, 2011, pp. 1–6.
- [6] T. Tsuji and M. Kaneko, "Estimation and modeling of human hand impedance during isometric muscle contraction," *ASME Dynamics Systems and Control Division*, vol. 58, pp. 575–582, 1996.
- [7] E. Burdet, R. Osu, D. W. Franklin, T. Yoshioka, T. E. Milner, and M. Kawato, "A method for measuring endpoint stiffness during multi-joint arm movements," *Journal of Biomechanics*, vol. 33, pp. 1705–1709, 2000.
- [8] E. J. Perreault, R. F. Kirsch, and P. E. Crago, "Effects of voluntary force generation, on the elastic components of endpoint stiffness," *Exp Brain Res*, vol. 141, pp. 312–323, 2001.
- [9] E. J. Perreault, R. F. Kirsch, and P. E. Crago, "Voluntary control of static endpoint stiffness during force regulation tasks," *J Neurophysiol*, vol. 87, pp. 2808–2816, 2002.
- [10] J. M. Dolan, M. B. Friedman, and M. L. Nagurka, "Dynamic and loaded impedance components in the maintenance of human arm posture," *IEEE Trans Systems, Man, and Cybernetics*, vol. 23, pp. 698–709, 1993.
- [11] T. Tsuji, P. G. Morasso, K. Goto, and K. Ito, "Human hand impedance characteristics during maintained posture," *Biol Cybern*, pp. 475–485, 1995.
- [12] M. C. Pierre and R. F. Kirsch, "Measuring dynamic characteristics of the human arm in three dimensional space," *Proceedings of the Second Joint EMBS/BMES Conference*, vol. 3, pp. 2558–2560, 2002.
- [13] R. D. Trumbower, M. A. Krutky, B.-S. Yang, and E. J. Perreault, "Use of self-selected postures to regulate multi-joint stiffness during unconstrained tasks," *PLoS one*, vol. 4, no. 5, p. e5411, 2009.

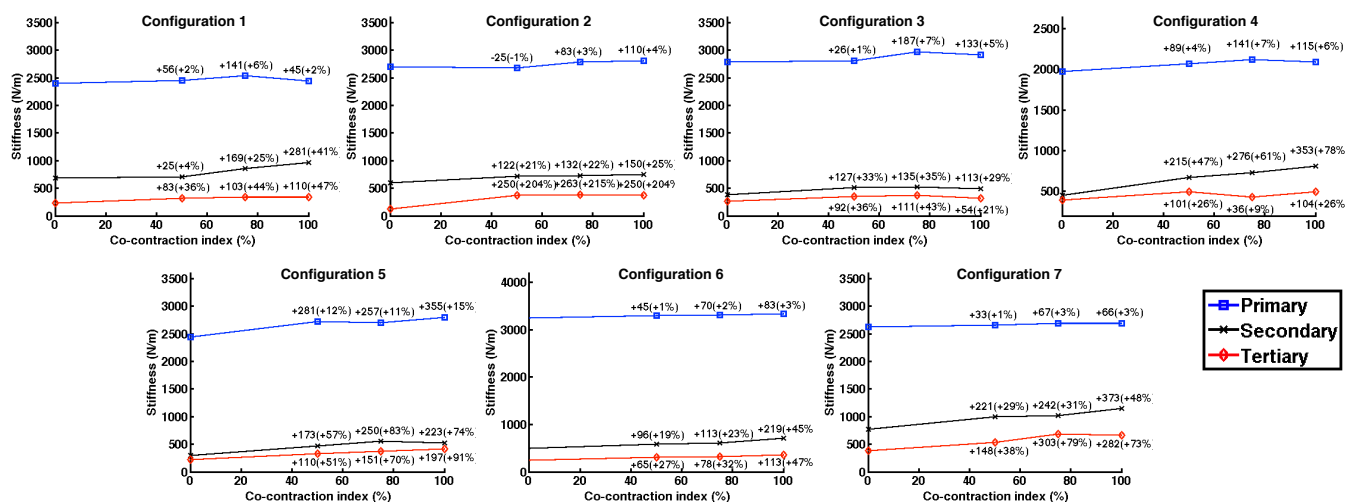


Fig. 6. Increase of the length of primary, secondary and tertiary axes of the stiffness ellipsoid with respect to muscle co-contraction index. Values are reported along the axes of the ellipsoid computed at the relaxed (0% co-contraction) case. Absolute difference and percentage is given for each case.

[14] M. A. Krutky, R. D. Trumbower, and E. J. Perreault, "Influence of environmental stability on the regulation of end-point impedance during the maintenance of arm posture," *Journal of neurophysiology*, vol. 109, no. 4, pp. 1045–1054, 2013.

[15] M. A. Krutky, V. J. Ravichandran, R. D. Trumbower, and E. J. Perreault, "Interactions between limb and environmental mechanics influence stretch reflex sensitivity in the human arm," *Journal of neurophysiology*, vol. 103, no. 1, pp. 429–440, 2010.

[16] T. Flash and F. A. Mussa-Ivaldi, "Human arm stiffness characteristics during the maintenance of posture," *Exp Brain Res*, pp. 315–326, 1990.

[17] R. Osu and H. Gomi, "Multijoint muscle regulation mechanisms examined by measured human arm stiffness and EMG signals," *J Neurophysiol*, vol. 81, pp. 1458–1468, 1999.

[18] R. Balasubramanian, R. D. Howe, and Y. Matsuoka, "Task Performance is Prioritized over Energy Reduction," *IEEE Transactions on Biomedical Engineering*, vol. 56(5), pp. 1310–1317, 2009.

[19] E. J. Perreault, R. F. Kirsch, and P. E. Crago, "Multijoint dynamics and postural stability of the human arm," *Experimental brain research*, vol. 157, no. 4, pp. 507–517, 2004.

[20] H. Gomi and R. Osu, "Task-dependent viscoelasticity of human multijoint arm and its spatial characteristics for interaction with environments," *J Neurosci*, vol. 18, pp. 8965–8978, 1998.

[21] D. W. Franklin, R. Osu, E. Burdet, M. Kawato, and T. E. Milner, "Adaptation to stable and unstable dynamics achieved by combined impedance control and inverse dynamics model," *Journal of neurophysiology*, vol. 90, no. 5, pp. 3270–3282, 2003.

[22] D. W. Franklin, U. So, M. Kawato, and T. E. Milner, "Impedance control balances stability with metabolically costly muscle activation," *Journal of neurophysiology*, vol. 92, no. 5, pp. 3097–3105, 2004.

[23] G. O'Neill, H. Patel, and P. Artemiadis, "An intrinsically safe mechanism for physically coupling humans with robots," in *Rehabilitation Robotics (ICORR), 2013 IEEE International Conference on*. IEEE, 2013, pp. 1–5.

[24] L. Sciavicco and B. Siciliano, *Modeling and control of robot manipulators*. McGraw-Hill, 1996.

[25] S. L. Campbell and C. D. Meyer, *Generalized inverses of linear transformations*. SIAM, 2009, vol. 56.



Harshil Patel received the B.Tech degree in mechanical engineering from Sardar Patel University, India, in 2009, and the M.S. degree in mechanical engineering from Arizona State University, Tempe, AZ, in 2013.

He was a Research Assistant at the Human-Oriented Robotics and Control Lab at Arizona State University. His research interests include robotics, human machine interfaces and rehabilitation robotics.



Gerald O'Neill received the B.S. degree in mechanical engineering from Arizona State University, Tempe, AZ, in 2013.

He was a Research Assistant at the Human-Oriented Robotics and Control Lab at Arizona State University. His research interests include robotics, human machine interfaces and exoskeletons.



Panagiotis Artemiadis received the Diploma and Ph.D. in mechanical engineering from National Technical University of Athens, Greece, in 2003 and 2009, respectively.

From 2009 to 2011 he was a Postdoctoral Research Associate at the Newman Laboratory for Biomechanics and Human Rehabilitation, in the Mechanical Engineering Department, Massachusetts Institute of Technology, Boston, MA. Since 2011, he has been with Arizona State University, where he is currently an Assistant Professor in the Mechanical and Aerospace Engineering Department, and director of the Human-Oriented Robotics and Control Lab. His research interests lie in the areas of robotics, control systems, system identification, brain-machine interfaces, rehabilitation robotics, neuro-robotics, orthotics, human motor control, mechatronics and human-robot interaction.

TABLE I
ARM STIFFNESS CHARACTERISTICS FOR 0% CO-CONTRACTION, AVERAGED ACROSS ALL SUBJECTS.

Configuration #	$\bar{K}_{xx} \pm (std)$ (N/m)	$\bar{K}_{yy} \pm (std)$ (N/m)	$\bar{K}_{zz} \pm (std)$ (N/m)	$\bar{K}_{max_A} \pm (std)$ (N/m)	$\bar{K}_1 \pm (std)$ (N/m)	$\bar{K}_2 \pm (std)$ (N/m)	$\bar{K}_3 \pm (std)$ (N/m)
1	524.2 ±56	987.1 ±25	1353.4 ±56	234.4 ±32	2182.2 ±94	654.2 ±51	175.7 ±46
2	245.2 ±82	2354.3 ±124	854.3 ±24	499.6 ±21	2698.2 ±71	651.2 ±86	137.1 ±14
3	491.1 ±65	2350.2 ±199	701.1 ±82	342.2 ±24	2756.2 ±99	402.5 ±23	201.1 ±45
4	801.3 ±99	1658.2 ±199	504.2 ±43	111.4 ±18	2041.5 ±24	651.2 ±99	451.2 ±43
5	605.1 ±83	2099.1 ±123	489.2 ±29	375.2 ±64	2420.2 ±198	475.2 ±44	287.2 ±41
6	401.2 ±41	2860.2 ±156	601.2 ±16	172.5 ±35	3198.1 ±89	502.2 ±72	237.2 ±52
7	679.2 ±76	2419.2 ±230	704.3 ±84	412.3 ±22	2487.6 ±26	803.2 ±78	346.2 ±67

TABLE II
ARM STIFFNESS CHARACTERISTICS FOR 50% CO-CONTRACTION, AVERAGED ACROSS ALL SUBJECTS.

Configuration #	$\bar{K}_{xx} \pm (std)$ (N/m)	$\bar{K}_{yy} \pm (std)$ (N/m)	$\bar{K}_{zz} \pm (std)$ (N/m)	$\bar{K}_{max_A} \pm (std)$ (N/m)	$\bar{K}_1 \pm (std)$ (N/m)	$\bar{K}_2 \pm (std)$ (N/m)	$\bar{K}_3 \pm (std)$ (N/m)
1	651.1 ±83	1177.1 ±131	1674.6 ±155	290.5 ±78	2421.0 ±312	799.6 ±221	282.2 ±110
2	559.9 ±132	2435.1 ±201	1021.5 ±103	492.4 ±74	2841.2 ±257	910.3 ±211	265.0 ±95
3	524.1 ±105	2406.1 ±226	829.1 ±194	378.8 ±72	2887.5 ±113	541.6 ±104	330.2 ±49
4	973.4 ±100	1766.3 ±169	654.6 ±101	113.3 ±20	2108.3 ±23	747.3 ±99	538.7 ±24
5	799.4 ±178	2243.3 ±215	613.4 ±34	356.6 ±86	2725.4 ±163	574.0 ±70	356.7 ±79
6	630.2 ±114	2927.0 ±240	775.6 ±165	213.1 ±56	3438.4 ±183	570.0 ±72	324.2 ±102
7	944.5 ±125	2432.1 ±175	900.8 ±164	375.1 ±45	2721.6 ±168	955.0 ±110	600.4 ±28

TABLE III
ARM STIFFNESS CHARACTERISTICS FOR 75% CO-CONTRACTION, AVERAGED ACROSS ALL SUBJECTS.

Configuration #	$\bar{K}_{xx} \pm (std)$ (N/m)	$\bar{K}_{yy} \pm (std)$ (N/m)	$\bar{K}_{zz} \pm (std)$ (N/m)	$\bar{K}_{max_A} \pm (std)$ (N/m)	$\bar{K}_1 \pm (std)$ (N/m)	$\bar{K}_2 \pm (std)$ (N/m)	$\bar{K}_3 \pm (std)$ (N/m)
1	451.8 ±114	1078.3 ±114	2144.3 ±215	293.3 ±18	2499.6 ±339	921.8 ±247	253.0 ±39
2	620.5 ±180	2516.1 ±156	1004.6 ±64	475.6 ±86	2928.7 ±310	894.3 ±223	318.1 ±112
3	602.7 ±67	2424.6 ±170	877.3 ±96	337.3 ±45	2949.5 ±145	585.7 ±155	369.4 ±83
4	987.5 ±117	1773.2 ±242	709.7 ±72	122.9 ±57	2132.0 ±86	755.6 ±143	582.6 ±172
5	790.2 ±102	2278.1 ±208	608.3 ±14	354.4 ±49	2731.3 ±181	582.1 ±87	363.5 ±80
6	676.8 ±140	2968.0 ±265	826.7 ±175	219.1 ±51	3518.9 ±68	590.9 ±43	361.0 ±76
7	1026.1 ±166	2441.9 ±111	943.2 ±87	350.8 ±515	2701.0 ±128	1022.4 ±102	686.9 ±49

TABLE IV
ARM STIFFNESS CHARACTERISTICS FOR 100% CO-CONTRACTION, AVERAGED ACROSS ALL SUBJECTS.

Configuration #	$\bar{K}_{xx} \pm (std)$ (N/m)	$\bar{K}_{yy} \pm (std)$ (N/m)	$\bar{K}_{zz} \pm (std)$ (N/m)	$\bar{K}_{max_A} \pm (std)$ (N/m)	$\bar{K}_1 \pm (std)$ (N/m)	$\bar{K}_2 \pm (std)$ (N/m)	$\bar{K}_3 \pm (std)$ (N/m)
1	595.9 ±91	1149.8 ±158	1985.1 ±197	318.1 ±48	2406.5 ±151	910.1 ±41	414.2 ±172
2	718.9 ±102	2502.8 ±138	1148.4 ±114	470.7 ±85	2924.1 ±246	1090.4 ±191	355.2 ±71
3	641.9 ±145	2423.5 ±191	844.2 ±98	334.4 ±73	2955.3 ±238	579.3 ±66	374.0 ±77
4	1076.9 ±99	1830.9 ±134	728.3 ±163	114.2 ±13	2182.5 ±160	845.5 ±187	608.0 ±91
5	831.3 ±254	2371.6 ±183	660.6 ±103	379.3 ±121	2827.8 ±65	642.2 ±118	393.4 ±31
6	725.3 ±98	3002.6 ±149	788.4 ±134	232.1 ±63	3471.0 ±150	627.6 ±91	417.7 ±124
7	1167.8 ±148	2476.4 ±169	915.5 ±146	339.6 ±52	2701.0 ±177	1191.2 ±105	667.5 ±92

TABLE V
ROTATION ANGLES OF THE PRIMARY, SECONDARY, AND TERTIARY AXES OF OF STIFFNESS ELLIPSOIDS FROM 0% TO 100% CO-CONTRACTION.

Configuration #	$\Delta\theta_1$ (°)	$\Delta\theta_2$ (°)	$\Delta\theta_3$ (°)
1	21.2	29.1	21.2
2	5.8	11.4	14.2
3	4.5	23.5	24.2
4	5.1	32.5	36.4
5	4.6	17.2	15.1
6	3.8	22.8	25.8
7	7.3	21.8	25.5